Mon. Not. R. Astron. Soc. **323**, 718–732 (2001)

Red synchrotron jets in Parkes quasars

M. T. Whiting,[1★] R. L. Webster[1] and P. J. Francis[2]†

[1]*Astrophysics Group, School of Physics, University of Melbourne, Victoria 3010, Australia*
[2]*Research School of Astronomy and Astrophysics, Australian National University, Canberra, ACT 0200, Australia*

Accepted 2000 December 13. Received 2000 November 13; in original form 1999 September 24

ABSTRACT

We present model fits to spectral energy distributions in the optical and near-infrared of >100 flat-spectrum radio quasars from the Parkes Half-Jansky Flat-spectrum Sample. We find that ~40 per cent of the sources have power-law spectral energy distributions (SEDs), while a similar number show evidence for two primary components: a blue power law and optical synchrotron emission. The blue power law is similar to the dominant component observed in the spectra of optically selected quasars. There is strong evidence that the synchrotron component has a turnover in the ultraviolet–optical rest frame of the spectrum. In the remaining sources, it is likely that the synchrotron peaks at longer wavelengths. This mixture of two components is supported by optical polarization measurements in a subgroup of the sources. The sources with power-law SEDs show evidence for an excess number of red power-law slopes compared with optically selected quasars. There are additional spectral components in some of the sources, such as dust and the underlying galaxy, which have not been considered here.

Key words: radiation mechanisms: non-thermal – BL Lacertae objects: general – galaxies: jets – quasars: general.

1 INTRODUCTION

The spectral energy distributions of active galactic nuclei (AGNs) provide a sum of the emission processes contributing to the energy output of the AGN. Clearly, several mechanisms contribute at most frequencies. If we can determine the different components as a function of frequency, then we can determine the energy generation mechanisms that are important.

Flat-spectrum radio quasars are known to be dominated in the radio spectrum by synchrotron emission. It is less clear how far these synchrotron spectra extend towards higher frequencies, or the magnitude of the contribution they make to the optical and near-infrared (NIR) spectrum – a region dominated by the Big Blue Bump.

The far-infrared emission of flat-spectrum quasars appears to be dominated by synchrotron emission (Haas et al. 1998), consistent with a Doppler-boosted component that swamps the expected emission from dust components. Synchrotron emission in the optical has been considered for many years to be necessary to explain the optical to NIR photometry of optically faint and red flat-spectrum radio quasars. This has mostly been on the basis of the steepness of the optical–NIR spectra (Rieke, Lebofsky & Kinman 1979; Beichmann et al. 1981; Bregman et al. 1981; Rieke, Lebofsky & Wiśniewski 1982). The steepness of these spectra suggested a cut-off, or sharp break, in the electron energy spectrum. Supporting evidence for the presence of synchrotron emission at NIR wavelengths comes both from the variability in the NIR, and from the strong polarization of a few sources. Stickel et al. (1996) found that variability was a general characteristic of optically faint flat-spectrum radio sources, although they did not specifically discuss synchrotron emission. Instead, they suggest that reddening due to intervening galaxies or the host galaxy itself was the likely cause of the red optical colours.

While radio jets are quite common, and have been widely observed, optical counterparts to these jets are quite rare. In fact, only 14 optical jets are currently known (see O'Dea et al. 1999, and references therein). The features (i.e. emission knots) in the optical jets match the positions of features in the radio jets, indicating that the emission regions and mechanisms for the two spectral regimes are associated. Optical jets can be used to put strong constraints on the particle energetics, by providing limits on the maximum energies, and on the acceleration mechanisms, because of the short lifetimes of particles at these energies (Meisenheimer, Röser & Schlötelburg 1996).

The quasars considered in this paper are selected from the Parkes Half-Jansky Flat-spectrum Sample (PHFS) (Drinkwater et al. 1997), which consists of 323 objects selected to be radio-loud ($S_{2.7\,\mathrm{GHz}} > 0.5$ Jy), and have a flat radio spectrum ($\alpha_{2.7/5.0} > -0.5$, $S(\nu) \propto \nu^{\alpha}$). These quasars have been shown (Webster et al. 1995; Francis, Whiting & Webster 2000a, hereafter FWW) to have

★ E-mail: mwhiting@physics.unimelb.edu.au
† Joint Appointment with the Department of Physics and Theoretical Physics, Faculty of Science.

a large spread in $B - K$ colours, with the reddest objects having $B - K > 7$. Masci, Webster & Francis (1998) showed that this spread could not be accounted for by the emission from the host galaxy.

In this paper we test the idea that optical synchrotron emission causes the red optical–NIR colours of the PHFS quasars. Models representing emission from both an optical synchrotron component and a blue optical power law (representing the continuum emission from an unreddened quasar) are fitted to broad-band optical–NIR spectra. Standard goodness-of-fit techniques are used to determine models that are consistent with the observations.

The data set was compiled by FWW, and comprises broad-band optical and NIR photometry in the bands *B*, *V*, *R*, *I*, *J*, *H* and *K*. This photometry is quasi-simultaneous, meaning that all observations for a given source were made within several days (six at most) of one another. This minimizes the effects of source variability. The source selection used for this paper is explained in Section 2. The simultaneity, as well as the breadth and density of the spectral coverage of this data set, provide an excellent basis to model the broad-band emission from a large number of flat-spectrum quasars.

The data set is described in Section 2. In Section 3 we test the hypothesis that the emission in the optical–NIR region is well fitted by a single power law. In Section 4 we describe the more sophisticated model that was fitted to the data – representing the accretion disc and synchrotron emission – and the method that was used to perform the fitting. The results of this fitting are described in Sections 5 and 6, while further tests of the model fits are examined in Section 7, using polarization and emission-line measurements. A possible rival model – that of blackbody emission by hot dust – is considered in Section 8. The effect of emission lines on the photometry and the resulting fits is investigated in Section 9. Finally, Section 10 contains discussion of the results and their implications.

2 DATA

The data that have been fitted by these models are described in detail in FWW. A total of 157 sources from the PHFS were observed, with quasi-simultaneous broad-band photometry observations in the bands *B*, *V*, *R*, *I*, *J*, *H* and *K*. These magnitudes were converted into broad-band fluxes using the zero-points given in the same paper.

2.1 Excluded sources

Not all sources in FWW were used. First, we only considered those sources with complete contemporaneous photometry in all bands, or those with only one observation missing (either not observed or an upper limit). This was to ensure that the number of degrees of freedom in the model fitting was greater than zero. Those sources with more than one band missing were not included in the analysis. Sources without a measured redshift were also excluded, since the redshift is needed to obtain the correct shape of the observed synchrotron spectrum. One of the sources that had an unknown redshift ($z = 0$) in Drinkwater et al. (1997), 0829+046, has a published redshift value of $z = 0.18$ (Falomo 1991), which is used here. Also excluded were low-redshift galaxies, which had a prominent 4000-Å break between the *B* and *V* bands. These sources show strong evidence for flux from the underlying galaxy in their spectra (Masci et al. 1998), and thus need an additional galactic component to be modelled accurately. Sources with $z > 3$ were also excluded, as these had strong Lyα breaks present between *B* and *V*. This reduced the number of sources from 157 to 117.

Twenty-one of the reddest sources ($B - K > 5$) in the subsample were amongst those excluded, as they have only upper limits on *B*, *V* and possibly *R*, or no redshift. The sources with upper limits are both red and optically faint. Since the flux of these sources typically decreases rapidly in the blue (i.e. from *V* to *B*), there are three possible explanations for them. They are either dust-reddened (causing the blue decrease in flux), high-redshift (and hence Lyα-absorbed), or dominated by synchrotron that turns over rapidly. Future analysis of the spectral energy distributions (SEDs) of these sources will only strengthen our final conclusions.

Those sources excluded purely because of their lack of measured redshift generally have high $B - K$ colours ($B - K > 5$), since the most likely reason they have no redshift is that they are faint in the optical (and in particular in the blue). Further discussion of the sources excluded from the sample is given in Section 10.

2.2 Errors on photometry

The photometry given in FWW quoted error bars, where the estimated error comprised two parts: a random error component and an assumed 5 per cent error in the photometric zero-points, which were added together in quadrature. The photometric zero-point errors were estimated from the scatter in zero-points between different standard star measurements in an individual night: FWW adopted a value of 5 per cent to account for this error.

However, this zero-point error ignores a number of factors that we believe may be important for the analysis in this paper. These factors are as follows:

(i) The optical zero-magnitude fluxes were taken from Bessell, Castelli & Plez (1998). These fluxes were derived for an A0 star, and so will be slightly incorrect for a quasar spectrum. This has the effect of introducing small colour terms into the photometry, the size of which will depend on the spectral index of the object being observed. A similar effect will of course be present in the NIR. Bersanelli, Bouchet & Falomo (1991) found that spectral shape differences could produce systematic errors of at least a few per cent in the NIR flux.

(ii) The zero-point fluxes in the optical are taken from a different reference (Bessell et al. 1998) from those in the NIR, which were calculated by P. McGregor (*CASPIR* manual, MSSSO, ANU), assuming that Vega is well represented in the NIR by a blackbody of temperature 11 200 K, and normalization $F_\lambda(555\,\mathrm{nm}) = 13.44 \times 0^{-12}\,\mathrm{W\,cm^{-2}\,\mu m^{-1}}$ (Bersanelli et al. 1991). These different zero-points may not be exactly equivalent, which will produce small offsets between the optical and NIR parts of the SED.

(iii) If the sky conditions at Siding Spring Observatory were not completely photometric for all observations for a given source (particularly if the transparency changed between different bands), then the measured photometry will have small band-to-band errors present.

(iv) The observations for each source were taken quasi-simultaneously (meaning all observations were made within at most a six-day period), to minimize the effects of variability. However, a number of the sources in the PHFS have been found to exhibit intra-day variability in the optical (Romero, Cellone & Combi 1999; Heidt & Wagner 1996), and a larger number no

doubt have similar properties to these. Therefore, variability on time-scales of the order of those separating our observations is likely for some of the sources. Such variability can be up to 0.1 mag over the period of a night.

(v) Finally, the presence of strong emission lines in the spectra of the quasars could boost the flux of a band above the level of the continuum. We have tried to quantify this effect in Section 9, although this is not possible to do for many sources, as a result of the lack of both photometry and a spectrum. Some additional effects may be due to line blends (such as Fe II blends), but this is probably not as strong an effect as you would find in a radio-quiet sample.

Hence, to take account of all these factors, we have increased the systematic error in the photometry to 10 per cent. The random error is kept at the same level as that presented in FWW, and is added in quadrature to the systematic error.

3 POWER-LAW MODEL

The object of our analysis is to find physical models to explain the optical and NIR emission. FWW found that about 90 per cent of the PHFS have approximately power-law SEDs. We first wish to test this more rigorously. As a starting point, we choose to fit (naively) a simple power law, with an unconstrained spectral index. This will separate out the sources that have power-law SEDs from those that show some curvature in their spectrum.

3.1 Fits to data

The model we choose to fit is $f_{\rm PL}(\lambda) = c\lambda^{\alpha}$, so that the normalization c and the spectral index α vary. (Note that this model implies $f_{\nu} \propto \nu^{-2-\alpha}$.)

This model is fitted to the data using a least-squares method. This generates a χ^2 value:

$$\chi^2 = \sum_{i=1}^{7} \frac{[y_i - f_{\rm PL}(\lambda_i)]^2}{\sigma_i^2},$$

which indicates the goodness of fit. A fit to a source will be deemed to be 'good' when the value of χ^2 is less than the cut-off value corresponding to the 99 per cent confidence level of the χ^2 distribution. For a source with five degrees of freedom (as is the case for most sources with this power-law model), this cut-off level is 15.09. (Note that increasing the value of this cut-off is equivalent to increasing the confidence level – for example, the 99.5 per cent cut-off is 16.75 for five degrees of freedom.) If the χ^2 value is greater than this cut-off level, then we reject the null hypothesis that the power-law model fits the data.

When we fit this power-law model to the data, we find that 83 sources (or 71 per cent of the total) have good fits. The distribution of resulting power-law indices, both for the good fits and for all sources, is shown in Fig. 1.

The spectral indices of these good fits span a wide range of values. At one extreme there are the sources with relatively blue SEDs ($\alpha \lesssim -1.4$). These sources are characterized by their blue continuum, the presence of moderate to strong emission lines, and generally low X-ray flux [most were not detected by *ROSAT* (Siebert et al. 1998)].

At the other extreme are the sources with redder SEDs (that is, flatter in f_{λ}), with $-1 \lesssim \alpha \lesssim 0$. These sources are blazar-type objects, with high optical polarization (Wills et al. 1992) as well as relatively weak (or even absent) emission lines – in fact, all the BL Lac objects in our sample are in this region.

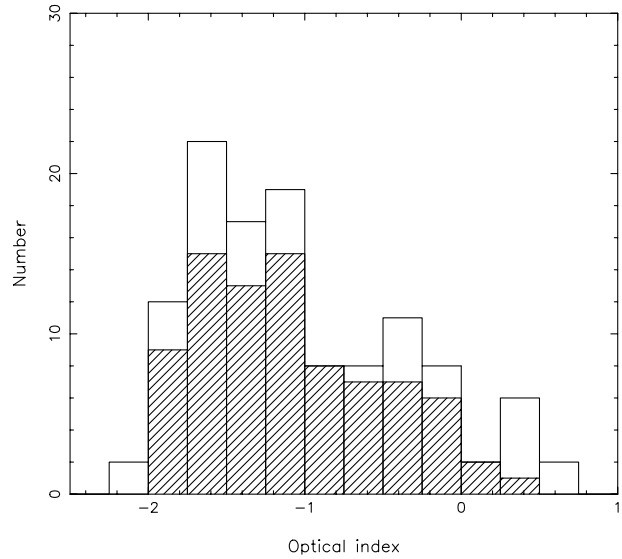

Figure 1. Histogram of fitted power-law indices. Hatched histogram indicates good fits, while open histogram indicates all fits.

3.2 Interpretation of power laws

So, we have fitted a power law to a large majority of the sources in our sample, spanning a wide range of spectral indices. Are the physical processes that generate this power law the same for all sources? That is, does the power law in the blue sources have the same origin as that in the red sources?

The first class of sources – the blue sources – are being fitted by a blue power law, which has similar colours to the blue power-law emission seen in optically selected quasars (Francis 1996). This is likely to be the optical part of the continuum emission from the accretion disc (often termed the Big Blue Bump).

However, the power law being fitted to the redder sources is most likely of different origin to that seen in the blue sources. These objects exhibit characteristics commonly associated with optical synchrotron emission (such as high optical polarization and lack of prominent emission lines), and so we postulate that this emission is, at least in part, some form of synchrotron emission. The slope of the power law can then be used to determine p, the power-law index of the electron energy distribution (i.e. defined such that $N(E) \propto E^{-p}$: see Section 4.2). Using the values shown in Fig. 1, we obtain $2 < p < 6$ (using $-1.5 < \alpha < 0.5$ and $p = 2\alpha + 5$).

If synchrotron emission is present in the spectra of at least some of these quasars, then we can ask the question, 'Is the synchrotron component best modelled by this power law?' The synchrotron component will be present in one of two forms: a power law caused by an unbroken (power-law) electron energy distribution, or a turning-over component caused by a break or a cut-off in the electron energy distribution. (Note that the power law can also be produced by a synchrotron spectrum turning over at higher frequencies than those observed.)

Both of these forms can be tested. The power-law model must produce power-law indices that are consistent with slopes of plausible energy distributions. The presence or otherwise of a turnover can be evaluated by examining the sharpest possible

turnover (caused by an abrupt cut-off in the energy distribution at some maximum energy). This will provide the maximum contrast with the power law, and is consistent with modelling done by other authors (Meisenheimer et al. 1996, for example).

Many of the sources, while they have power-law fits that we cannot reject at the 99 per cent confidence level, show evidence for curvature in their SEDs. This curvature can be 'n'-shaped (higher in the middle than at either end), 'u'-shaped (lower in the middle) or perhaps take the form of an inflection (e.g. the flux decreases, levels off and decreases again). (See Fig. 3 for illustrations of the different types.) Most of the sources classed as BL Lac objects are 'n'-shaped, and so we postulate that these sources are dominated by a synchrotron component that is turning over in the optical.

Other sources, however, are bluer in the optical than in the NIR (i.e. show an inflection, without the turn-up seen in 'u'-shaped sources). This is a possible indication of the presence of excess emission in the NIR, in addition to a blue power law. We propose that this excess emission is due to a synchrotron component that has turned over in the NIR, and so does not dominate in the optical, where the dominant emission is instead a blue power law similar to that observed in the bluest sources.

4 PHYSICAL MODELS

In response to this phenomenological classification, we propose the following physical model. There are two components in this model: one is a blue power law, representing continuum emission from the accretion disc region; and the second is synchrotron emission, representing emission from the relativistic jet (that we know to be present because of the flat-spectrum radio emission seen in these objects).

4.1 Accretion disc emission

We find, from the simple power-law fitting, that the bluest sources have power-law continua. The slopes of these power laws are consistent with them being the same component as that seen in optically selected quasars, commonly termed the Big Blue Bump (BBB). We take this component to represent the underlying quasar continuum in the ultraviolet–optical part of the rest-frame spectrum – that is, the 'unreddened' quasar continuum.

Over the wavelength of our observations, the BBB is modelled as a simple power law, $f_\lambda \propto \lambda^{\alpha_B}$ or $f_\nu \propto \nu^{-2-\alpha_B}$. Francis (1996) found that the median slope for a subsample of quasars from the Large Bright Quasar Survey (LBQS), taken from optical/NIR photometry, was $f_\nu \propto \nu^{-0.35\pm0.3}$, and noted that the observations were consistent with an intrinsic continuum slope of $f_\nu \propto \nu^{-0.3}$ that is reddened by various amounts of dust. We therefore take our value of α_B to be -1.7. The effects of allowing the value of α_B to vary are considered in Section 10.

4.2 Synchrotron emission

All the PHFS sources are radio-loud flat-spectrum sources, and thus very likely have relativistic jets that emit synchrotron radiation, at least at radio frequencies. Could this synchrotron emission extend up to the optical/NIR part of the spectrum? Our power-law fitting from the previous section provides circumstantial evidence for this: the redder sources in the optical tend to be the ones with higher polarization (a good sign of synchrotron emission) and less prominent emission lines (possibly a sign that the emission lines are being swamped by the presence of a synchrotron component). These pieces of evidence are investigated more deeply in Section 7.

As discussed above, the synchrotron spectrum could take the form of either a power law, from a power-law distribution of electron energies, or a power law with a break or turnover, due to an electron energy distribution that exhibits a break or even a cut-off. This latter type of spectrum has been seen in optical synchrotron jets (O'Dea et al. 1999; Scarpa et al. 1999), where the optical spectrum is like $\nu^{-1.2}$–$\nu^{-3.0}$, compared to a radio–optical spectrum of $\nu^{-0.6}$–$\nu^{-1.0}$.

Additionally, a synchrotron spectrum that has a turnover will, when combined with the blue power law, be able to reproduce an inflection-like SED. Such a spectrum, particularly in the region of the turnover, will also be quite red, thus accounting for the red colours of many of the SEDs.

4.2.1 *Analytic modelling*

We consider here synchrotron emission from a population of electrons with an energy distribution with the form of a power law up to some maximum energy and zero beyond this (i.e. an energy spectrum with an abrupt cut-off). This can be expressed as a distribution of the Lorentz factor γ of the radiating electrons:

$$N(\gamma)\,\mathrm{d}\gamma \propto \begin{cases} \kappa\gamma^{-p}\,\mathrm{d}\gamma & 1 \le \gamma \le \gamma_c, \\ 0 & \gamma > \gamma_c. \end{cases}$$

This is consistent with modelling done by Meisenheimer et al. (1996) on the jet of M87. They found that the overall synchrotron spectrum of the brightest parts of the jet was best described by a spectrum that had a sharp cut-off at $\nu_c \approx 10^{15}$ Hz, with an energy distribution of the form of a straight power law $N(\gamma) \propto \gamma^{-2.31}$, with a rather abrupt high-energy cut-off. We consider the effect of using a power-law synchrotron spectrum instead in Section 10.

Such a synchrotron spectrum is straightforward to model analytically. We use the 'classical' synchrotron model, as first calculated by Schwinger (1949), and as derived by a number of authors, particularly Pacholczyk (1970) and Longair (1994), whose derivation we follow.

The single-particle luminosity for a radiating electron (mass m_e, charge e, Lorentz factor $\gamma = E/m_e c^2$, and pitch angle, or angle between trajectory and magnetic field direction, θ) in a uniform magnetic field B is given by

$$L_{1p}(\omega) = \frac{\sqrt{3}e^3 B \sin\theta}{8\pi^2 \epsilon_0 c m_e} F(x),$$

where $\omega = 2\pi\nu$ is the angular frequency,

$$x = \frac{2\omega\beta m_e}{3\gamma^2 e B \sin\theta}$$

and $F(x)$ is defined in terms of the Bessel function $K_{5/3}(z)$ by

$$F(x) = x\int_x^\infty K_{5/3}(z)\,\mathrm{d}z.$$

We are interested in the luminosity of a population of particles, so we need to integrate $L_{1p}(\omega)$ over suitable distributions of energies and pitch angles. The energy distribution is that given above, while the pitch angle distribution that we use is an isotropic one, where the probability distribution is $p(\theta)\,\mathrm{d}\theta = \frac{1}{2}\sin\theta\,\mathrm{d}\theta$.

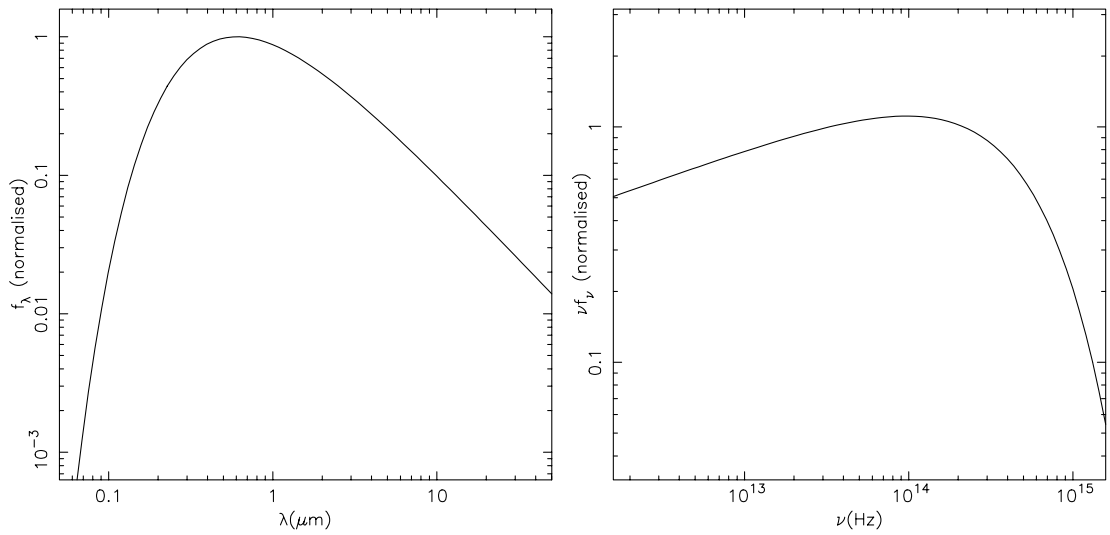

Figure 2. The synchrotron model used in the analysis, in both f_λ and νf_ν units. Both plots have been normalized so that the peak flux in f_λ is 1. Note that the vertical scale is different in the two plots.

Thus, the integrated luminosity from such a population is

$$L(\omega) = \frac{\sqrt{3}e^3 B\kappa}{16\pi^2\epsilon_0 c m_e}\int_0^\pi \sin^2\theta\left[\int_1^{\gamma_c}\gamma^{-p}F(x)\,\mathrm{d}\gamma\right]\mathrm{d}\theta.$$

An example of such a spectrum is shown in Fig. 2, for $\gamma_c = 10^4$ and $B = 10^{-4}$ T = 1 G (the value of κ has been taken to be 1). The peak frequency ν_c depends on these two values, and can be shown by simple arguments (Blandford 1990) to be approximated by $\nu_c \sim \gamma_c^2 B$ MHz (where B is measured in gauss).

The slope of the power-law tail (at frequencies $\nu \ll \nu_c$) is related to the energy power-law index by $\alpha_S = (p-5)/2$ (where $f \propto \lambda^{\alpha_S}$). The energy distribution for the spectrum in Fig. 2 is taken to be $N(\gamma) \propto \gamma^{-2.5}$ (i.e. $p = 2.5$), giving a power law of $f_\lambda \propto \lambda^{-1.25}$.

We consider here a range of p values from $p = 2.0$ to $p = 3.0$, which gives a range of long-wavelength power-law slopes of $\alpha_S = -0.5$ to $\alpha_S = -1.0$. This range covers the distribution of radio-to-optical slopes observed in optical synchrotron jets (Scarpa & Urry 1999). Allowing p to vary does not significantly alter the results of our analysis – see Section 10 for further discussion.

We also note here that a value of $p > 3$ means that the νF_ν flux will increase towards longer wavelengths (since $F_\nu \propto \nu^{-(p-1)/2}$ and so $\nu F_\nu \propto \nu^{-(p-3)/2}$), and this results in the radio flux being severely overestimated by the fitted synchrotron component, since the radio emission always has a lower $\nu F\nu$ flux than the optical. [This assumes that the same synchrotron component is responsible for both the optical and radio emission, which is an assumption commonly made, particularly for the modelling of optical synchrotron jets (Meisenheimer et al. 1996).]

4.3 Model fitting

These two components (the blue power law and the synchrotron component) are combined linearly to form a model $f_C(\lambda) = a\lambda^{-1.7} + bf_{\mathrm{synch}}(\lambda)$ that is fitted to the data in the same way as the power-law model (that is, using χ^2 minimization). The reduced χ^2 value (that is, χ^2/ν) for each of the two models (combined and power law) are compared, and the model with the lowest χ^2/ν is chosen to be the best-fitting model.

In fitting the combined model, the location of the peak wavelength of the synchrotron spectrum, λ_p, was allowed to vary. This variation was allowed to occur over a range of rest-frame wavelengths such that the curvature of the spectrum caused by the turnover affected the synchrotron flux in the region of the data points (in other words, we did not want to be fitting just the power-law part of the synchrotron spectrum). Quantitatively, we took the minimum peak wavelength to be half a decade shorter than the B band (0.44 μm) shifted to the rest frame. We then considered twenty λ_p values per decade (evenly spaced in $\log_{10}\lambda_p$), up to a maximum peak of 10 μm. For each of these synchrotron functions, a best fit to the data was found, and then the best of these was chosen, giving the best-fitting λ_p value for that source.

5 RESULTS FOR PHYSICAL MODELS

This combined model was fitted to the photometry, and compared to the power-law fits. The best-fitting model was chosen on the basis of the lowest reduced χ^2 value, as described above. For the default values of the parameters ($p = 2.5$ and $\alpha_B = -1.7$), we find that 93 sources (or 79 per cent of the total) are well fitted by one of the models. Of these, 48 are fitted best by the power-law model, and 45 by the combined model. How these numbers change with different parameter values is discussed in Section 10.4. A selection of the fits are shown in Fig. 3, for a range of power-law slopes and synchrotron peak wavelengths.

We note here that, although there are 48 sources fitted best by the power-law model, many of these have combined fits that are only slightly worse than the power-law fit. This indicates that there is not a great deal of difference between the fits of the two models. This is not the case with the combined model sources, as for most of these the combined model fit is a lot better than the power-law fit.

A histogram of χ^2/ν values is shown in Fig. 4, with the distributions for the two different models shown separately. The distribution for the sources fitted best by the combined model is noticeably broader than that for the power-law sources, with more sources having very low χ^2 values.

While many sources have been fitted better with the combined model, a large number are still preferentially fitted with the power

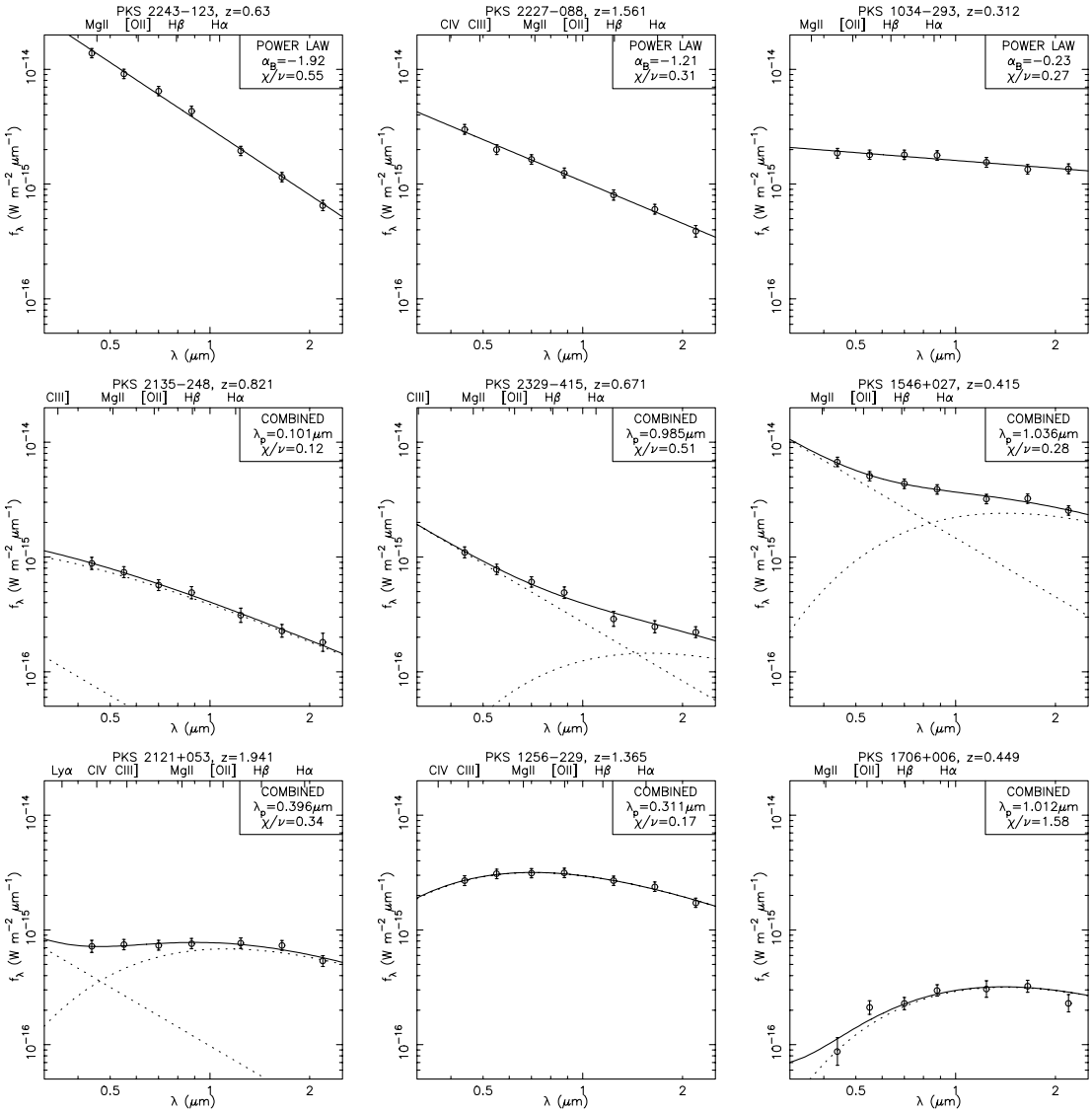

Figure 3. Examples of the various types of photometry, and the fits to them. The horizontal axis on each plot is wavelength, in μm, and the vertical axis is f_λ, in $\mathrm{W\,m^{-2}\,\mu m^{-1}}$. The locations of notable emission lines are shown, based on the redshift of each quasar. For the combined fits, the individual components – the power law ($\alpha_\mathrm{B} = -1.7$) and the synchrotron component ($p = 2.5$) – are shown as dotted lines. The λ_p value, where given, is for the quasar rest frame. A full compilation of the fits to all the quasars in the sample is given in Whiting (2000).

law. If we plot a histogram (Fig. 5) of the power-law indices of those still fitted by the power-law model, we can see that those sources that are preferentially fit by the power-law model are the bluer sources, while the majority of the sources with indices $\alpha > -1$ are fitted better by the combined model.

6 FITTED SYNCHROTRON COMPONENTS

The properties of the synchrotron components that are fitted as part of the combined model are of particular interest. As can be seen in Fig. 6, the peak wavelengths are restricted to a relatively narrow range of values (approximately a decade in wavelength). However, this is likely to be largely a reflection of the distribution of the wavelengths of the photometric points.

The strength of the fitted synchrotron component varies considerably from source to source. In Fig. 7, the ratio of the synchrotron and power-law components at a rest-frame wavelength of 0.5 μm is shown for all sources fitted best by the combined model. The main bulk of this distribution spans nearly four orders of magnitude. This large range of values, which is also seen in the normalizations of the individual components, indicates that we are seeing a continuum of variations of these components, probably as a result of variations in the strengths of the inner jet and emission from the accretion disc and/or surrounding regions.

We also note that a small number of the sources at the high-ratio end of the distribution are faint, red sources, which are likely to be significantly dust-reddened. They are thus fitted with a dominant synchrotron component, as the synchrotron spectrum has the approximate form of a power law with an exponential cut-off (which is the same as a power law with dust extinction).

7 TESTING THE FITS

7.1 Polarization

We have shown that a large fraction of the sources in the PHFS

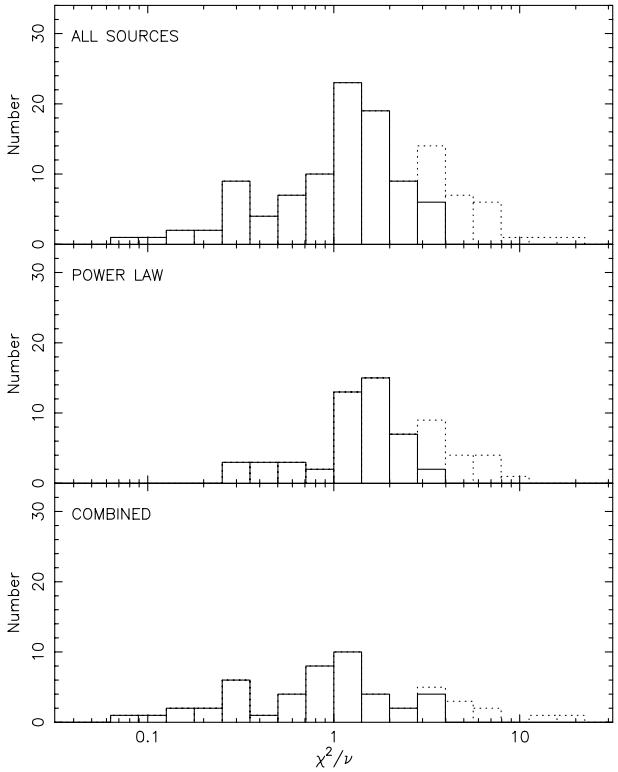

Figure 4. Histograms of the reduced χ^2 values, for all sources and for each of the best-fitting models. The dotted histogram shows those sources whose fits are rejected at the 99 per cent confidence level.

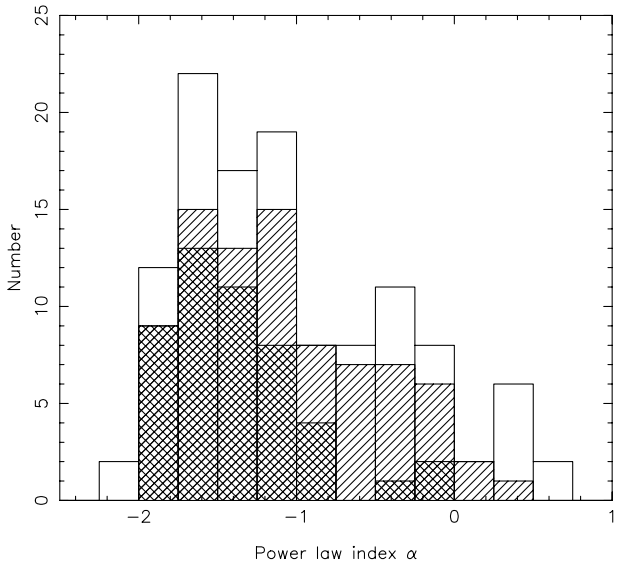

Figure 5. Distributions of the fitted power index α. The open histogram shows the results of the power-law fit to all 117 sources; the hatched histogram shows which sources have a power-law fit accepted at 99 per cent confidence; while the cross-hatched histogram shows which of those sources have power-law fits better than the combined fit.

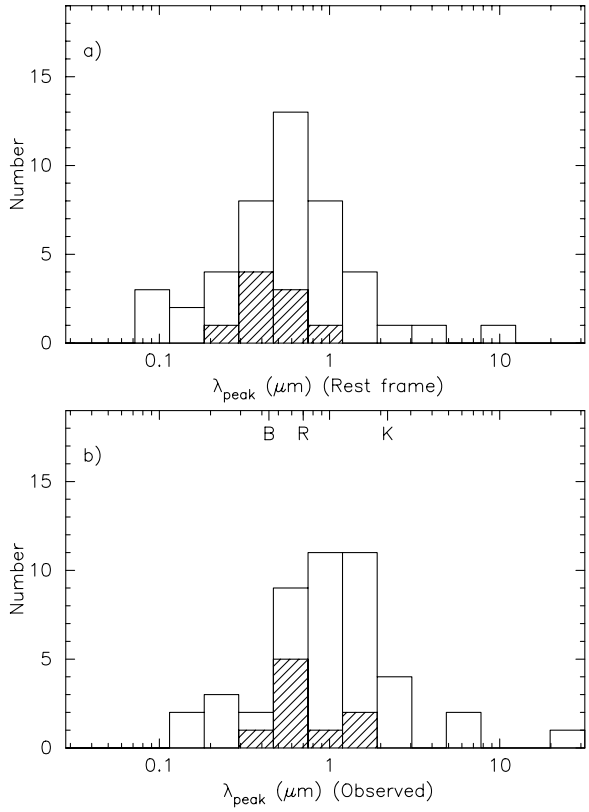

Figure 6. Histogram of peak wavelengths, showing all sources fitted best with the combined model, in (a) the rest frame, and (b) the observed frame. The solid histograms show all sources accepted at 99 per cent confidence, while the hatched histograms show the BL Lac objects. The locations of three prominent emission lines and photometric bands are given for reference.

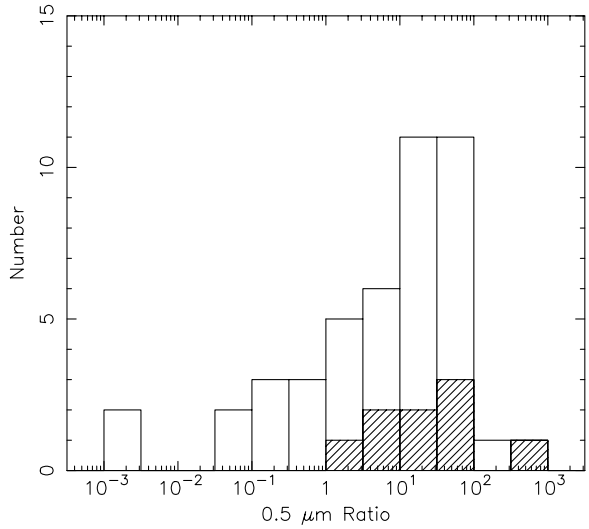

Figure 7. Histogram of ratios of the synchrotron component to the power-law component of the combined model, for those sources fitted best by the combined model. The ratio is calculated at a rest-frame wavelength of 0.5 μm. The hatched histogram shows the BL Lac objects.

show evidence for the presence of optical synchrotron emission, where the amount of synchrotron emission present in the spectrum changes with wavelength. How else can we test this model? One of the key features of synchrotron radiation is its high degree of polarization. If there is significant synchrotron emission at optical and NIR wavelengths, then one would expect to be able to detect a corresponding polarization. Indeed, this has been used as a way to confirm the presence of synchrotron emission in optical jets [Baade (1956) provided the first example of this for the jet of M87.]

In our combined model, the synchrotron component is the only polarized component, as we assume that the BBB component, which is essentially emission from the accretion disc, is unpolarized [$P < 1$ per cent for the BBB (Antonucci 1988)]. Thus, the amount of polarization will depend on the proportion of the total flux that is due to the synchrotron emission. Furthermore, if the relative amount of synchrotron emission changes with wavelength, as it does with the models we have fitted, then the amount of polarization should also change with wavelength.

Such dependences have been investigated previously by a number of different authors, for samples that include some sources considered here. Wills et al. (1992) studied a large sample of bright, flat-spectrum core-dominant quasars, measuring their optical polarization. An interesting result is that they found that the fraction of quasars with $P > 3$ per cent in a fixed observed passband decreased with increasing z, possibly indicating that the percentage polarization decreases towards shorter rest-frame wavelengths. This would be consistent with the presence of a synchrotron component turning over in the optical region.

Impey & Tapia (1990) present radio and optical data for a slightly larger sample of radio-selected quasars, including optical polarization measurements. They find strong statistical links between strong optical polarization and properties such as compact radio structure, superluminal motion and weak emission lines. They explain this by requiring the optical emission, as well as the compact radio emission, to be relativistically beamed.

Smith et al. (1988) obtained multicolour (*UBVRI*) polarization measurements of 11 highly polarized quasars, and found that three of these exhibited decreasing polarization towards shorter wavelengths, which they modelled as a combination of polarized synchrotron emission and two unpolarized components, from the broad-line region and the accretion disc. None of these sources, however, are part of our sample.

7.1.1 *Optical polarization*

First, we wish to compare our model predictions with published optical polarization measurements. We use the large catalogue of measurements compiled by Wills et al. (1992). We want to compare these measurements with the fractional amount of flux due to the fitted synchrotron component. However, since the observations of Wills et al. were made without a filter, we have determined the average synchrotron fraction by integrating over the range 0.3–1 μm.

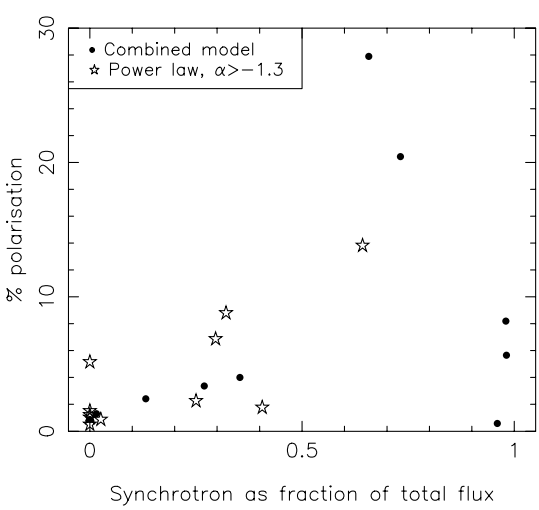

Figure 8. Polarization from Wills et al. (1992) as a function of the proportion of the total flux made up by synchrotron. The sources are given different symbols according to the nature of their best-fitting model.

We have then plotted in Fig. 8 the percentage polarization as a function of this average synchrotron fraction. For those sources that were fitted best by the power-law model, we have calculated the fraction from the combined model fit, and indicated these sources by a different symbol. All the power-law sources with polarization measurements had relatively red power-law indices (i.e. $\alpha > -1.3$).

The spread in polarization measurements at large synchrotron fractions is much greater than at low fractions, indicating that the high-polarization sources generally have large amounts of synchrotron fitted to them (at the wavelengths at which the polarization is measured). Additionally, all but one of the sources at zero (or near-zero) synchrotron fraction have low optical polarization.

The two exceptions to this picture are 1020−103 and 0202−172. First, 1020−103 has a very high synchrotron fraction (∼95 per cent), but has very little optical polarization ($P = 0.58$ per cent). In this case, the source has a power-law continuum with a slight curvature, which is fitted well by an almost pure synchrotron curve. It may be that this curvature is due to effects other than synchrotron, which explains the lack of polarization. A possible candidate is contamination from the very strong Hα line, which would boost the continuum level in the centre of the SED.

Secondly, 0202−172 has a measured polarization of 5.15, but also has a very blue power-law continuum ($\alpha = -1.85$). This continuum slope is possibly too steep to attribute to synchrotron (it implies a value of $p = 1.3$ – in turn implying a rather flat energy distribution). However, the location of the synchrotron peak may have shifted in the period since the polarization measurements were made (the polarization measurements were taken 8 yr prior to our photometry observations).

7.1.2 *Near-infrared polarization*

To try to avoid the problem of non-simultaneity of the photometry and polarization observations, we obtained polarization measurements of eight quasars in the NIR, using the IRIS instrument on the Anglo-Australian Telescope. The details and results of the observations will be presented elsewhere (Whiting et al., in preparation). These measurements are nearly simultaneous with the photometry measurements (a difference of ∼40 d), and so can be directly related to the fitted components. The wavelength dependence of the polarization can then provide an important test on the models we are fitting.

Since the synchrotron component is the only polarized component, one would expect the percentage polarization to be directly related to the amount of synchrotron flux present, and, in fact, the percentage polarization will be directly proportional to the ratio of synchrotron flux to total flux. In Fig. 9, we have plotted the polarization of each of these quasars as a function of wavelength, and, on the same plot, the synchrotron ratio normalized (arbitrarily, as it is the wavelength dependence we are interested in, not the precise normalization) to the longest-wavelength polarization point (which is usually the *K*-band point). For completeness, we also show a line of constant polarization, normalized to the *K*-band point. All these sources are fitted best with the combined model, with the exception of 1101−325, which is fitted best by the power-law model (its SED taking the form of a

blue power law, $\lambda^{-1.81}$). We have used the combined model fit to it for the purposes of Fig. 9.

We have also included polarization measurements from Wills et al. (1992) where they exist. Again, these are put at an observed wavelength of 0.5 μm. Note, of course, that these points are not simultaneous with the NIR points.

The fitted synchrotron component generally replicates well the wavelength dependence of the polarization, although for some sources, such as 1313−333, the points are equally well given by a constant-polarization component. This is what you would expect from a pure synchrotron component, and these sources are typically BL Lac objects, from which you would expect to see a synchrotron-dominated SED. A notable exception to this is 0537−441, whose polarization is not well fitted by a constant synchrotron component, but is fitted better by a combination of a synchrotron and a significant power-law component. However, it is apparent from these plots that having simultaneous optical polarization measurements would better help to discriminate between the combined model and a constant-polarization model.

7.2 Emission lines

Synchrotron flux emitted from the PHFS quasars is most likely to come from a thin, relativistic jet, and the radiation will not be isotropic. This means that there will be very little synchrotron radiation directed towards the emission-line clouds, which have a much larger covering angle. Thus, the ionization of these clouds will be due to the continuum emission from the central accretion disc region – in other words, the Big Blue Bump.

One might expect that adding a non-ionizing synchrotron component to the continuum will have the effect of reducing the equivalent width of the emission lines from the broad-line region, because the flux in the emission lines is not changed but the continuum flux is increased.

To test this prediction, we compared the equivalent widths of five emission lines (C IV 1549, C III] 1909, Mg II 2798, Hβ and the doublet [O III] 4959,5007) with the ratio of synchrotron to continuum flux at the line wavelength, to see if some form of an anticorrelation is present. The details of the observations are presented elsewhere (Francis et al. 2001). Objects that had spectra taken were essentially a random sample of the PHFS (subject to visibility during the observing run).

In Fig. 10, we show the results of this comparison for the Mg II and Hβ lines, which are the two broad lines with the longest wavelength (and hence the two lines most likely to show a reduction in equivalent width). We have also plotted those sources best fitted with the power-law model. The value of the ratio used for these sources was taken from fitting the combined model, and so are upper limits to the ratio.

The Mg II line does not show much relationship to the synchrotron ratio, while the Hβ line does show a reduction in equivalent width with increasing amount of synchrotron. This

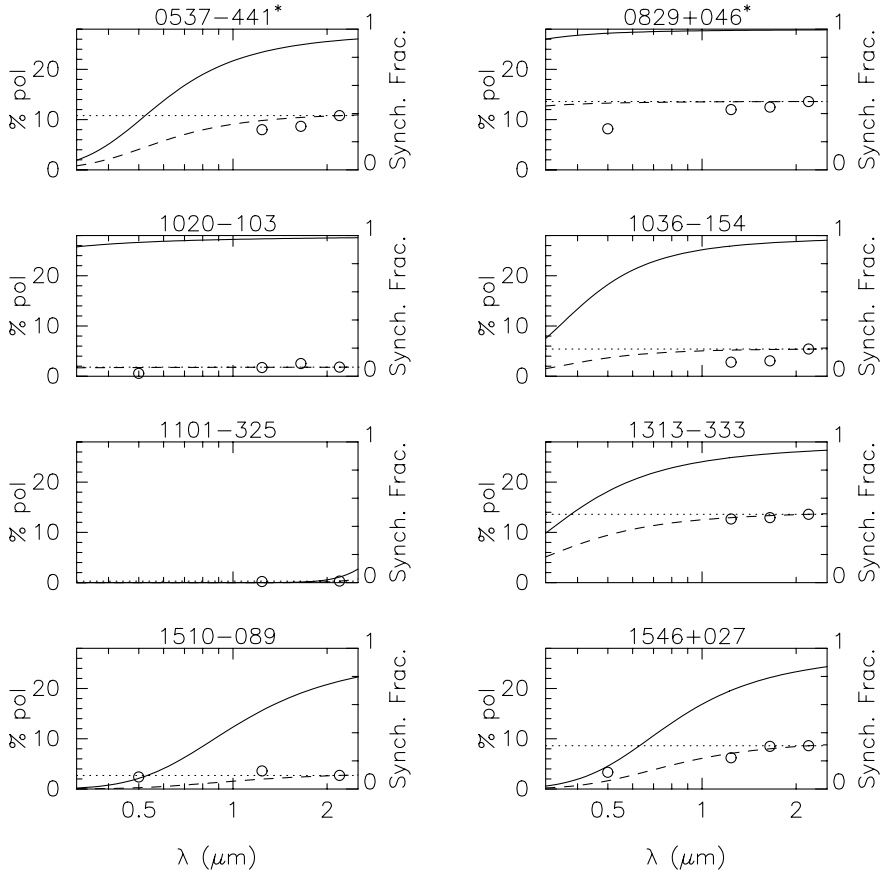

Figure 9. Near-infrared polarization of a selection of quasars as a function of wavelength. Also shown are optical measurements from Wills et al. (1992). The solid lines show the fraction of the total flux made up by the synchrotron component (right-hand axis), while the dashed line shows this normalized (see text) to the *K*-band data point, and is in polarization units (left-hand axis). The dotted line shows constant polarization, normalized to the *K*-band data point as well. A * denotes that the object is a BL Lac.

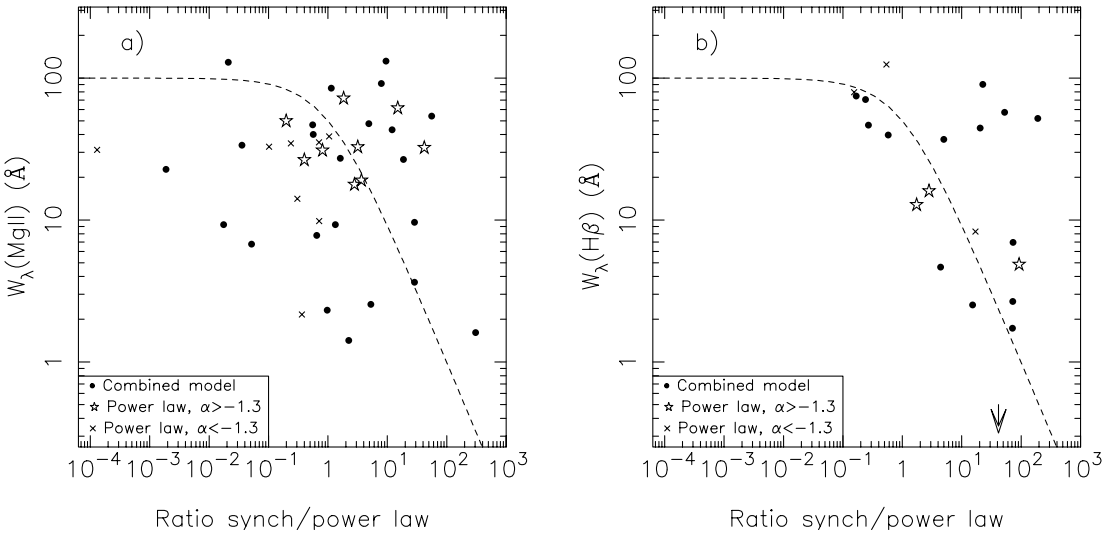

Figure 10. The equivalent width of (a) the Mg II and (b) the Hβ lines as a function of the ratio of synchrotron to continuum flux at the emitted wavelengths. The sources are given different symbols according to the nature of their best-fitting model (the arrow indicates an upper limit for a source that was fitted best with the combined model). Ratios for sources fitted best by the power-law model are calculated from the combined model fits, and so are upper limits to the ratios (for the crosses and stars). The dashed lines represent the expected change in equivalent width with increasing amount of synchrotron, for an emission line with intrinsic equivalent width of 100 Å.

lends some support to the hypothesis that excess synchrotron light is present. The difference in the two plots is probably due to the presence of the turnover in the synchrotron flux, so that it has less effect at the shorter wavelength of Mg II. There are, however, several sources that have high synchrotron ratios together with high equivalent widths. The implications of these results are discussed in Section 10.

8 HOT DUST: AN ALTERNATIVE TO SYNCHROTRON?

So far, we have shown that, for a number of sources, the optical–NIR photometry is well fitted with a power law plus a curved component, which we have assumed to be the turnover of a synchrotron component. However, could another model be used instead of synchrotron? One possible alternative is blackbody emission resulting from hot dust.

To test this model, we used a blackbody emission spectrum due to dust at a temperature of 1750 K [the sublimation temperature characteristic of dust grains consisting of graphite and silicates (e.g. Laor & Draine 1993)] emitted in the rest frame of the quasar. A blackbody curve at this temperature would have its peak, in the quasar rest frame, at 1.66 μm. This blackbody spectrum was combined with the same $\lambda^{-1.7}$ power law used in the combined model to produce a model that was fitted to the data.

The fits generated by this model were almost always worse than those of the synchrotron model. This was due to the peak of the blackbody occurring at much longer observed wavelengths than the K band. In only 12 cases was the χ^2/ν value from the dust model less than that of the synchrotron model, and in most cases this was because the dust model had one more degree of freedom. For each of these objects, the SED took the form of a blue power law (one object was $\lambda^{-1.4}$, and the rest were bluer than $\lambda^{-1.54}$) that had a slight amount of reddening at the H and K bands, which was fitted by the presence of the dust blackbody curve. For the majority of the sources, however, the hot dust model was a lot worse than the synchrotron model, and so cannot provide the peak in the optical/NIR that is required to explain many of the observed SEDs.

A number of authors (Sanders et al. 1989, for example) have argued for the existence of a NIR bump, somewhere around 3 μm, corresponding to blackbody emission from hot dust. Sanders et al. (1989) also mention the presence of a local minimum at 1 μm, which they note for its 'universality'. They interpret this to be due to the finite sublimation temperature of dust, causing a drop in the blackbody emission, combined with the rise in flux of thermal emission from hot ($T \gtrsim 10\,000$ K) gas.

Any dip observed in our data occurs at wavelengths that are too short to be attributed to hot dust. To observe a 1-μm dip, we would need photometry at longer wavelengths.

9 EFFECT OF EMISSION LINES ON PHOTOMETRY

As mentioned in Section 2, the presence of a strong emission line in the wavelength range of one of the filters will raise the SED level above that of the continuum, which will increase the systematic error in the photometry.

To test this effect, and to see how the fits to the photometry are affected, we examined several sources whose spectra showed significant emission lines. To calculate the contribution of the emission line, we define the total flux in the line as $F_{\rm line}$ and the total continuum flux *under* the line as $F_{\rm cont}$. Then the change in magnitude is given by

$$\Delta m = 2.5\log_{10}\left(\frac{F_{\rm line}+F_{\rm cont}}{F_{\rm cont}}\right) = 2.5\log_{10}\left(\frac{\Delta\lambda + W_\lambda}{\Delta\lambda}\right),$$

where W_λ is the equivalent width of the line, and $\Delta\lambda$ is the wavelength range over which the flux is measured. The equivalent widths and fluxes were computed using the SPLOT routine in IRAF.

Note that we are only able to do this analysis for a small number of sources, as we do not have spectra for all sources, and those

spectra that we do have are often of poor quality, and in almost all cases non-simultaneous.

The values of the change in magnitude, when considered over the same wavelength range as that of the broad-band filters ($\Delta\lambda \sim$ 1000–2400 Å for the optical bands), ranged from 0.05 to 0.25 mag. By artificially reducing the flux in the relevant band by this amount, we could evaluate the change in χ^2 caused by the presence of the emission line. This was done for several sources that had strong emission lines present in their spectra [the spectra for a large number of PHFS sources will be presented elsewhere (Francis et al., in preparation)]. A few specific examples are as follows:

(i) 1510−089 has a strong Hα line in the *I* band ($\Delta m = 0.14$), as well as a combination of a strong Hβ line and prominent Fe II emission in the *R* band ($\Delta m = 0.11$). The removal of flux corresponding to these lines caused a reduction in χ^2/ν of nearly 50 per cent (from 1.28 to 0.68), without greatly changing the resultant fit, although the fitted synchrotron peak was at a slightly longer wavelength.

(ii) 1725+044, similarly, has Hα in *I* band ($\Delta m = 0.13$) and Hβ + [O III] in *R* band ($\Delta m = 0.07$), and removal of these more than halves χ^2/ν from 2.49 to 1.17, without changing the location of the peak of the synchrotron.

(iii) 1036−154 has a large Mg II line in the *B* band ($\Delta m =$ 0.17), which causes a noticeable upturn in the SED. Removal of this line reduces the χ^2/ν from 0.77 to 0.56, without changing the location of the peak wavelength, although the 0.5-μm ratio increases slightly (from 5.3 to 7.2).

(iv) 1136−135 is initially fitted with a pure power law, and this remains the case after removal of the Mg II line ($\Delta m = 0.09$ in *B*) and both the Hβ and the strong [O III] (total $\Delta m = 0.11$ in *I*). The power-law index softens slightly (from −1.85 to −1.81) and the χ^2/ν value decreases from 0.43 to 0.29.

In conclusion, by selecting quasars with strong emission lines, we have demonstrated that the largest changes to the SED are $\Delta m \sim 0.25$ in one waveband. In most of the cases investigated, removal of the line flux improved the χ^2/ν value, but did not significantly alter the nature of the fit. When good-quality long-wavelength spectra (preferably at least quasi-simultaneous with the photometry, which is not the case here) are available for these quasars, it should be possible to recalculate the fits, taking the emission-line contributions into account, although we do not expect the general conclusions to change.

10 DISCUSSION

10.1 Types of source

The fitting of a single power law to the photometry, as detailed in Section 3, separates the sources into classes depending on the goodness of the power-law fit and the value of the spectral index. The combined model fits have refined this description so that we are able to talk about the different types of sources present in the sample.

First, the bluest sources are all fitted with the power-law model, and are generally consistent with being the same type of sources as optically selected quasars. The power-law model also best fits a number of objects of intermediate slope ($\alpha \sim -1.2$), as well as a few red sources ($\alpha > -0.5$). These latter sources, as seen in Section 7.1, are generally high-polarization sources, and so are likely to be synchrotron-dominated – they of course show no evidence for a turnover similar to that being fitted by the synchrotron model, although their slope could be due to a very steep energy distribution (i.e. large *p*) or a more gradual turnover.

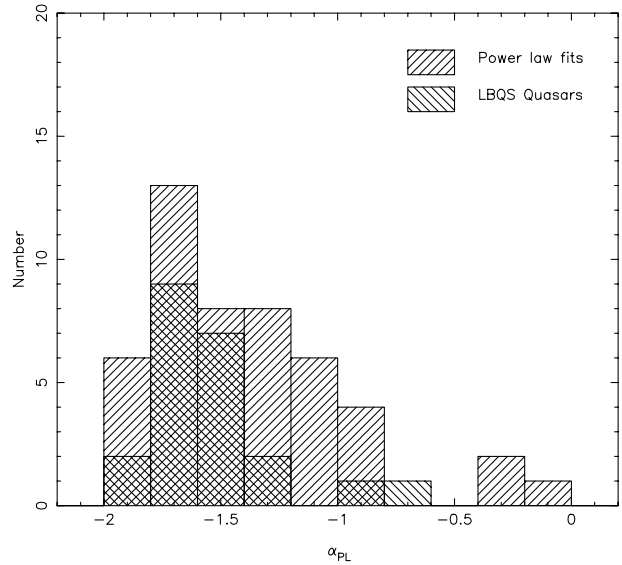

Figure 11. Histograms of power-law indices for the power-law sources in this paper and for the LBQS quasars from Francis (1996).

The presence of the intermediate power-law slopes raises interesting issues. Do we see similar sources in optical quasar surveys? In Fig. 11, we have plotted the power-law index distributions for the sources best fitted by the power-law model, as well as the LBQS quasars from Francis (1996). While we cannot say that the two data sets come from different parent distributions (the Kolmogorov–Smirnov test probability for the null hypothesis that the parent distributions are the same is 11.3 per cent), there does appear to be an excess of quasars in our sample for $-1.4 \lesssim \alpha \lesssim -0.8$. This may indicate that the accretion disc emission in radio-loud quasars has a broader range of colours, which would have implications for models of accretion disc emission.

The power-law sources, like all sources in the PHFS, have a radio synchrotron component. The peak of this component may be at longer wavelengths than those covered by our observations, i.e. in the IR. This would be consistent with observations of flat-spectrum radio quasars in the far-infrared (Haas et al. 1998). These longer-wavelength peaks would be due to lower-energy emitting particles, and would therefore constitute the extension of the energy distribution, of which we see the high-energy end in the two-component sources. To test this assertion, one needs to obtain observations at longer wavelengths than the *K* band. We are in the process of obtaining observations of a number of sources at *L* band, and the results will be published and discussed at a later date.

Secondly, the combined model generally best fits the redder sources, although some intermediate sources are also fitted, particularly those with SEDs that show inflections. The synchrotron components fitted to the photometry of these sources all peak in the rest-frame optical and NIR.

Thirdly, the other category of sources are those that are optically faint. These sources all decrease in flux towards shorter wavelengths (indeed, some are not detected in the *B* band), and we suggest that these sources are heavily dust-reddened. We note that an exponentially reddened power law has the same form as the synchrotron component we are fitting, and these sources are fitted by a combined model with a dominant synchrotron component.

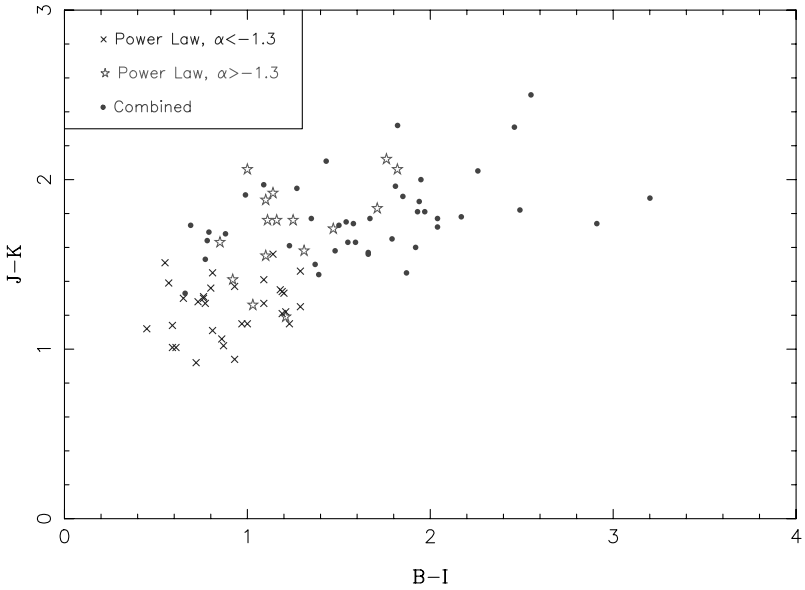

Figure 12. Infrared ($J - K$) colour versus optical ($B - I$) colour for all quasars with good model fits. The best-fitting model is indicated by the symbol used.

Table 1. Fitting results for sources that were excluded from the sample purely as a result of their undetermined redshift. The best-fitting model is given along with either the peak synchrotron wavelength (for combined fits) or the power-law index (for power-law fits). $F_{0.5}$ denotes the fraction of the total flux made up by the synchrotron component, at an observed wavelength of 0.5 μm. Note that a * denotes a $V - K$ measurement, not $B - K$, since a B measurement was not made (because of the faintness of the source in B).

Source name	B (mag)	$B - K$	Best-fitting model	α	λ_p (μm)	$F_{0.5}$	Good/bad fit
0048−097	16.12	3.61	Combined	–	0.15	0.97	Good
1110−217	24.41	7.67	Combined	–	1.85	0.88	Good
1156−094	21.95	5.08	Combined	–	1.04	0.69	Good
1648+015	21.87	5.31	Combined	–	1.17	0.82	Bad
1732+094	$B > 23.5$, $V = 21.15$	>7.13	Power law	−0.39	–	0.00	Bad
2056−369	$V > 23.5$, $R = 23.45$	>5.39*	Power law	0.59	–	0.00	Good
2245+029	21.71	6.22	Combined	–	1.85	0.41	Good
2337−334	22.93	6.54	Power law	0.36	–	0.00	Good
2344−192	23.52	6.27	Combined	–	1.65	0.83	Bad

Finally, we can check the consistency of our model fits by plotting the sources on a colour–colour diagram. In Fig. 12 we plot the $J - K$ colours of all sources against the $B - I$ colours – that is, the infrared colour against the optical colour. We separate the sources into their fitted model types, separating the power-law sources by their fitted slope (using $\alpha = -1.3$ as the dividing line).

Clear distinctions can be made between the different model types. The blue power-law sources lie at the bottom left corner, indicating blue colours in both optical and infrared, while, as the power law becomes redder, the sources move towards the upper right. Many of the combined fits are in the optically red region of the plot, indicating that the SED is turning over in the optical (similar to 1256−229 in Fig. 3, for example). The reddest sources in $B - I$ are sources with optical continua that drop towards the blue, in the manner of 1706+006 (see Fig. 3), which are typical of dusty sources, or sources dominated by host-galaxy emission, and are fitted by a dominant synchrotron component. Note that 1706+006 is the faintest of the sources shown in Fig. 3, and so is a good candidate for dust extinction. Other combined sources, however, are among the bluer sources in the optical, but have redder NIR colours than the power-law sources. These are the sources that show an inflection, similar to 1546+067 in Fig. 3, where the synchrotron component is dominant in the NIR but turns over and has less effect in the optical.

10.2 Sources excluded from the sample

As explained in Section 2, there are a number of sources that were excluded from the sample. Some of these were excluded for the sole reason that they did not have a measured redshift. These sources were generally quite red and optically faint (thus explaining their undetermined redshift), with the exception of the BL Lac object 0048−097, which has a power-law SED. We fitted our models to the observed wavelengths of these objects, to investigate the bias created by excluding them. Note that this fitting does not take into account the change in shape of the synchrotron spectrum due to the redshift of the source. The results are summarized in Table 1.

As can be seen, all but three of the sources are fitted with the combined model, and the three that are not are fitted with quite red power laws. The location of the peak wavelengths are generally into the NIR, which are longer than the bulk of the distribution of the sources with redshifts (see Fig. 6). Also, the synchrotron component that is fitted is generally fairly dominant, as evidenced by the fraction values $F_{0.5}$. However, it is unlikely that many of these sources would truly be synchrotron sources as they show more the characteristic shape of dust absorption and are quite faint in the optical (again, with the exception of 0048−097, which was fitted with the power-law tail of a dominant synchrotron model).

Table 2. Number of sources fitted best by each model. Only those fits accepted at the 99 per cent confidence level are shown. Values of the parameters used are $p = 2.0$, $p = 2.5$ and $p = 3.0$, as well as $\alpha_B = -1.4$, $\alpha_B = -1.7$ and $\alpha_B = -2.0$.

p	2.0	2.0	2.0	2.5	2.5	2.5	3.0	3.0	3.0
α_B	−1.4	−1.7	−2.0	−1.4	−1.7	−2.0	−1.4	−1.7	−2.0
Power law	46	44	45	49	48	48	53	52	52
Combined	49	51	50	44	45	44	39	40	40
Total	95	95	95	93	93	92	92	92	92

We propose that these sources are dust-dominated rather than synchrotron-dominated.

10.3 Sources without good fits

Up to this point, we have only discussed the results for the sources with good (i.e. acceptable at the 99 per cent confidence level) fits. A total of 24 sources (or 21 per cent of the total) are not fitted well by either the power-law model or the combined model. What sort of sources are these?

A few sources (∼8) have roughly power-law SEDs, but with a little curvature ('n'-shaped) in the blue end of the optical. This may be indicative of a small amount of dust attenuation or extinction.

Most of the other sources have one or more photometric points that do not smoothly connect with the rest of the SED. It is possible that, for these points, at least one of the systematic errors discussed in Section 2.2 is dominating, over and above the level we assigned. In some sources, there may also be further emission processes present that we have not modelled.

10.4 Alternative values of p and α_B

Throughout this paper, we have used values for the electron energy index of $p = 2.5$, and for the BBB spectral index of $\alpha_B = -1.7$. We consider here the effect that changing these values has on the results. In Table 2, we list the numbers of sources best fitted by each of the two models, for each set of parameters, as well as the total number of sources fitted by one of the models.

Reducing the value of p means that the synchrotron spectrum has a bluer slope, which enhances the effect of the turnover. Using a lower value of p in the combined model results in some sources, otherwise fitted by the power law, being instead fitted by the combined model. This is indeed seen in Table 2, where the number of sources fitted by a power law decreases as you move from $p = 3$ to $p = 2.5$ to $p = 2$ (if the value of α_B is kept constant), while the number of sources fitted by the combined model increases. Note also that more sources have good fits for the lower values of p.

The λ_p distributions are also affected by a changing p value. For lower p values, there are more sources with shorter λ_p values (that is, close to 0.1 μm). This is the result of the slope of the power-law tail of the synchrotron spectrum: for higher p values the slope is redder, and so such a synchrotron spectrum peaking around 0.1 μm would contribute too much at the longer wavelengths.

For the spectral index of the blue optical power law used in the combined model, we considered both steeper and flatter values than the one mentioned in Section 4.1. The dispersion found by Francis (1996) for the slopes of LBQS quasars is $\pm \sim 0.3$, and so we consider here slopes in f_λ of $\alpha_B = -1.4$ and $\alpha_B = -2.0$.

Changing the slope of this power law (while keeping p constant) has a much less drastic effect than changing the value of p. As the slope becomes steeper in f_λ (that is, bluer), we see that only a couple of sources fitted by the power law change to be fitted by the combined model. The distribution of λ_p values is not changed considerably by the variation of the α_B values.

In summary, reasonable changes to the fiducial values of α_B and p make little difference to the fits, both in the λ_p distribution and the numbers fitted by each model, although the difference will be accentuated if the values of α_B and p are both taken to extremes.

10.5 Nature of synchrotron model

Thus far, we have been considering a synchrotron model that peaks at some λ_p and then turns over sharply (i.e. exponentially). The reasons we chose this were for consistency with other modelling done for optical synchrotron emission (Meisenheimer et al. 1996), and to provide the maximum contrast with the power-law model. However, synchrotron emission could alternatively be present in the form of a power law. What if we have a model of the same form as the combined model, but with this power-law synchrotron model instead? Is this any better at fitting the observations?

We constructed such a model, being a linear combination of the blue (BBB) power law from earlier, and a power law of variable index: $f(\lambda) = a\lambda^{-1.7} + b\lambda^{\alpha_S}$. To distinguish it from the BBB power law, we restricted the indices to the range $-1.6 < \alpha_S < 1.5$. This model was then fitted to the photometry in the same way as previously. Note that the special case of $a = 0$ is simply the power-law fit from Section 3 (with the index restricted to lie in the above range).

The χ^2/ν values for this model are plotted in Fig. 13 against those for the combined model detailed in Section 4. The symbols used indicate which model is preferred, and whether it is a good or bad fit. For sources that are bluer than $\lambda^{-1.7}$, the best fit is always with no synchrotron component (for both forms of the synchrotron model), as the presence of the second component will redden the blue power law. Hence, for these sources, both the original combined model and the two power-law models give the same fit, consisting of just the $\lambda^{-1.7}$ (i.e. BBB) power law. These sources are indicated by the 'Equal' symbols on Fig. 13.

The power-law synchrotron model obviously does not do as well at explaining the optical/NIR SEDs of the quasars as the model with a turnover. Only 22 sources have a good power-law synchrotron fit that is better than their fit from the synchrotron model with a turnover, and only two of these (1034−293 and 2329−415, with indices of $\alpha_S = -0.21$ and $\alpha_S = 0$ respectively) are significantly better. These power-law synchrotron sources may have turnovers at shorter wavelengths, beyond our currently available data. The only way to tell would be to obtain UV photometry (ideally contemporaneous with the optical/NIR).

We note that many of the sources from Fig. 5 that are in the

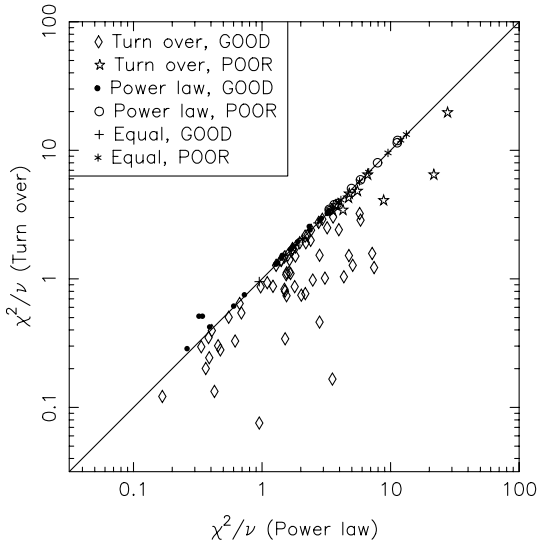

Figure 13. Values of χ^2/ν for the combined models featuring either power-law synchrotron models or synchrotron models with a turnover. The symbols relate to which model is preferred, and whether the fit is accepted at the 99 per cent confidence limit or not (i.e. good or poor). The line shown is the line of equal χ^2/ν.

cross-hatched histogram (that is, had better single power-law fits than combined fits) and had $\alpha > -1.6$, also had fits with the two power-law model that were better than those with the turnover synchrotron model. (This is not always the case, however, since going from one power law to two decreases the degrees of freedom, so the χ^2/ν value will be greater.) In most of these cases, the blue power law (the $\lambda^{-1.7}$ component) is either absent or has a very low normalization.

For most sources, however, the synchrotron model with a turnover gives a much better fit to the observed optical/NIR SEDs (many of these sources show large ratios of synchrotron to blue power-law flux). This result provides clear evidence that there is a break or a cut-off present in the energy distribution of the radiating particles.

10.6 Emission lines and BL Lac objects

We can use the results of the emission-line study in Section 7.2 to draw some conclusions about BL Lac objects, which are noted for having very small or non-existent emission lines. This is usually explained by the presence of a beamed synchrotron component from a jet directed towards us (Blandford & Rees 1978, for example). The results shown in Fig. 10 seem to support this explanation, as the equivalent widths tend to decrease with increasing amount of fitted synchrotron, as you would expect if there was an extra synchrotron component over the top of the emission lines.

Also, the fits to the BL Lacs in our sample are suggestive of strong synchrotron components. All nine BL Lacs are well fitted by the combined model, and the 0.5-μm ratios of the synchrotron to power-law components range from 3 (0537−441) to over 700 (1256−229) (see Fig. 7). These ratios, on average, are higher than the rest of the population (although it is only a small group).

However, there may be more to the story. As can be seen from Fig. 7, there are a number of sources with comparable ratios to the BL Lacs. Also, Fig. 10 shows signs of a large dispersion in the equivalent width distribution, particularly at the high-ratio end, with sources present that have relatively high ratios at the emission lines in question, as well as large equivalent widths. Perhaps there are other factors that determine whether an object is a BL Lac or not. One factor that is likely to be important is the strength or dominance of the emission-line region, with BL Lacs having an intrinsically weak emission-line flux. Such an idea agrees with other studies: for example, Ghisellini et al. (1993) found that BL Lac objects had significantly lower Doppler factors than core-dominated quasars. This was interpreted as suggesting that BL Lac objects have intrinsically weaker emission lines than core-dominated quasars.

11 CONCLUSIONS

The results of this paper can be summarized in the following conclusions:

(i) Radio-loud quasars require one of at least two components to fit the rest-frame optical SEDs. These two components are well modelled by an optical power law, which in some sources is similar to the blue power law seen in optically selected quasars, and a synchrotron component that turns over in the range $0.1\ \mu\mathrm{m} \lesssim \lambda_\mathrm{p} \lesssim 3\ \mu\mathrm{m}$.

(ii) The model fits require the synchrotron component to have a break or turnover at some wavelength λ_p in the observed wavelength range. A synchrotron spectrum with this break gives a much better fit to the data than a pure power-law synchrotron model. The value of λ_p provides strong constraints on the modelling of particle acceleration and emission mechanisms.

(iii) There is more than four orders of magnitude variation in the ratio of the synchrotron component to the power-law component in those sources fitted by the combined model. All the sources identified as BL Lacs lie at the high end of the distribution.

(iv) The fitting procedure is robust to reasonable changes in the values of the model parameters. The fits are statistically consistent with the data.

(v) There may be an excess of red power-law sources compared to optically selected quasars. This will have implications for emission models of accretion discs.

(vi) Sources that are well fitted by power laws have a synchrotron component that may peak in the IR. In the optical, these sources may be similar to optically selected quasars.

(vii) Optical polarization measurements (taken from the literature) support the synchrotron model fits to the SEDs.

(viii) There is some evidence for the equivalent widths of emission lines being reduced by the presence of the synchrotron component. This supports the hypothesis that BL Lac objects have a dominant synchrotron component, although other effects may contribute to the lack of emission lines in BL Lacs.

(ix) The red component fitted to the data, which has a turnover at some peak wavelength, cannot be hot dust. Emission from hot dust cannot peak at $\lambda_\mathrm{rest} < 1.66\ \mu\mathrm{m}$ as is required by our data.

(x) The red sources excluded from our analysis may provide interesting examples of extreme sources in the sample, e.g. very dusty sources, high-redshift sources, etc.

ACKNOWLEDGMENTS

MTW acknowledges the generous help of the Grimwade Scholarship from the University of Melbourne for assistance in carrying out this research. Thanks are due to Frank Masci for use of some of the polarization data prior to publication, and to the referee

(Patrick Leahy) for some very useful comments that improved the paper.

REFERENCES

Antonucci R. R. J., 1988, in Kafatos M., eds, Proc. 3rd George Mason Astrophysics Workshop, Supermassive Black Holes. Cambridge Univ. Press, Cambridge, p. 24
Baade W., 1956, ApJ, 123, 550
Beichmann C. A., Neugebauer G., Soifer B. T., Wootten H. A., Roellig T., Harvey P. M., 1981, Nat, 293, 711
Bersanelli M., Bouchet P., Falomo R., 1991, A&A, 252, 854
Bessell M. S., Castelli F., Plez B., 1998, A&A, 333, 231
Blandford R. D., 1990, Active Galactic Nuclei, Saas-Fee Advanced Course. Springer, Berlin, p. 161
Blandford R. D., Rees M. J., 1978, in Wolfe A. N., eds, Pittsburgh Conference on BL Lac Objects. Univ. Pittsburgh Press, Pittsburgh, p. 328
Bregman J. N., Lebofsky M. J., Aller M. F., Rieke G. H., Aller H. D., Hodge P. E., Glassgold A. E., Huggins P. J., 1981, Nat, 293, 714
Drinkwater M. J. et al., 1997, MNRAS, 284, 85
Falomo R., 1991, AJ, 102, 1991
Francis P. J., 1996, PASA, 13, 212
Francis P. J., Whiting M. T., Webster R. L., 2000, PASA, 17, 56 (FWW)
Francis P. J., Drake C. L., Whiting M. T., Drinkwater M. J., Webster R. L., 2001, PASA, submitted
Ghisellini G., Padovani P., Celotti A., Maraschi L., 1993, ApJ, 407, 65
Haas M., Chini R., Meisenheimer K., Stickel M., Lemke D., Klaas U., Kreysa E., 1998, ApJ, 503, L109
Heidt J., Wagner S. J., 1996, A&A, 305, 42
Impey C. D., Tapia S., 1990, ApJ, 354, 124
Laor A., Draine B. T., 1993, ApJ, 402, 441
Longair M. S., 1994, High Energy Astrophysics, Vol. 2, 2nd edn. Cambridge Univ. Press, Cambridge
Masci F. J., Webster R. L., Francis P. J., 1998, MNRAS, 301, 975
Meisenheimer K., Röser H.-J., Schlötelburg M., 1996, A&A, 307, 61
O'Dea C. P., De Vries W., Biretta J. A., Baum S. A., 1999, AJ, 117, 1143
Pacholczyk A. G., 1970, Radio Astrophysics. W.H. Freeman, San Francisco
Rieke G. H., Lebofsky M. J., Kinman T. D., 1979, ApJ, 232, L151
Rieke G. H., Lebofsky M. J., Wiśniewski W. Z., 1982, ApJ, 263, 73
Romero G. E., Cellone S. A., Combi J. A., 1999, A&AS, 135, 477
Sanders D. B., Phinney E. S., Neugebauer G., Sorfer B. T., Matthews K., 1989, ApJ, 347, 29
Scarpa R., Urry C. M., 1999, Proc. Life Cycle of Radio Galaxies Workshop, in press, New Astron. Rev.
Scarpa R., Urry C. M., 2001, Proc. Life Cycle of Radio Galaxies Workshop. New Astron. Rev., in press
Scarpa R., Urry C. M., Falomo R., Treves A., 1999, ApJ, 526, 643
Schwinger J., 1949, Phys. Rev., 75, 1912
Siebert J., Brinkmann W., Drinkwater M. J., Yuan W., Francis P. J., Peterson B. A., Webster R. L., 1998, MNRAS, 301, 261
Smith P. S., Elston R., Berriman G., Allen R. G., Balonek T. J., 1988, ApJ, 326, L39
Stickel M., Rieke G. H., Kühr H., Rieke M. J., 1996, ApJ, 468, 556
Webster R. L., Francis P. J., Peterson B. A., Drinkwater M. J., Masci F. J., 1995, Nat, 375, 469
Whiting M. T., 2000, PhD thesis, Univ. Melbourne
Wills B. J., Wills D., Breger M., Antonucci R. R. J., Barvainis R., 1992, ApJ, 398, 454

This paper has been typeset from a TEX/LATEX file prepared by the author.